Urban network traffic state estimation using a data-based approach

Martin Rodriguez-Vega, Carlos Canudas de Wit, Hassen Fourati

Urban network traffic state estimation using a data-based approach ⋆

Martin Rodriguez-Vega * **Carlos Canudas-de-Wit** *
Hassen Fourati *

* *Univ. Grenoble Alpes, CNRS, GIPSA-Lab, Grenoble INP, INRIA,*
38000 Grenoble, France. (e-mail: {martin.rodriguez-vega,
carlos.canudas-de-wit, hassen.fourati}@gipsa-lab.fr).

Abstract: In this paper we propose an estimator of vehicle density in every road section of a large urban traffic network. We assume a limited number of flow and turning ratio sensors can be installed, and that aggregate floating car data (FCD) is available, such that the space-mean speed of each road can be estimated. We propose a method to locate turning ratio sensors, which takes as input previous low-quality estimates of the turn rates, and then assigns to each intersection a weight according to the effect on the total density reconstruction error caused by perturbations between a priori and actual turning ratio values. We evaluate the models and estimator using data from the urban traffic network of Grenoble in France.

Keywords: Traffic density estimation, Sensor location, Large networks, Turning ratios.

1. INTRODUCTION

Traffic state estimation (TSE) is an important stage in the development of Intelligent Transportation Systems (ITS), as the knowledge of the evolution of traffic state variables such as flow and density for each road can be used to implement control strategies, or help in the decision taking stages for network design for better smart cities. This information can be used to calculate the mean traveling times for users, fuel consumption and vehicle emissions (important for air quality assessment), estimate the life of pavement, and many other applications. Because of this, accurate TSE is an active field in the transportation research literature [Seo et al. (2017)].

According to Rostami Shahrbabaki et al. (2020), two main components of existing estimation methods are the modeling choice and the input data. The most commonly used model for traffic dynamics is the well-known Lighthill-Whitham [Lighthill and Whitham (1955)] and Richards [Richards (1956)] (LWR) model, and its discrete counterpart, the Cell Transmission Model (CTM) [Daganzo (1994)]. This model is based on the vehicle conservation law, in addition with a empirical relationship between road density and traffic flow known as the Fundamental Diagram. In Highways, this approach for traffic state estimation is extensively used as in Tampère and Immers (2007), Mihaylova et al. (2007), Canudas de Wit et al. (2012), Canepa and Claudel (2017) and more recently in Takenouchi et al. (2019). The case of networks, requires additional modeling tools to describe vehicle interactions in intersections, Jabari (2016). The extended version of the CTM developed in Daganzo (1995) brings a solution

this problem via a flow maximization formulation under constraints provided by the fundamental diagram. This approach is widely used as can be seen in Lovisari et al. (2016) and Ladino et al. (2018).

However, the use of the fundamental diagram, specially in urban networks, is challenging as it requires the calibration of many parameters. Moreover, the presence of external factor such as traffic lights and pedestrian crossings, contradict the hypothesis of the LWR model that vehicle speed is only a function of its local density. Thus, data-based approaches that do not require a fundamental diagram have been proposed. The main tool in many methods, is to use probe vehicle that periodically send information about traffic conditions such as speed and headway, as showed in Bekiaris-Liberis et al. (2016), Wright and Horowitz (2016) for Highways and Rostami Shahrbabaki et al. (2020) in networks. These methods show promising results, but in some applications individual traces of probe vehicles might not be available due to privacy regulations.

In addition to these approaches, developments in new sensing technologies make available new information sources that can be used in TSE approaches. Abbott-jard et al. (2013); Bhaskar and Chung (2013) proposed the use of WiFi and Bluetooth scanners for the evaluation of traffic conditions, and for the estimation of road traveling times. Another data source are mobile phone networks, which have been studied by Derrmann et al. (2020); Li et al. (2020). Moreover, GPS traces of probe vehicles, also known as Floating Car Data (FCD) [Treiber and Kesting (2013)] can be more easily obtainable as they can be ensured to protect user privacy.

Our contribution in this paper is the proposal of a data-based traffic state estimation method for general urban networks that requires little knowledge of input parameters. We make use of three different data sources: station-

ary flow sensors, vehicle and FCD. Data provided by these sources is used to estimate the external inflows to a traffic network, the turning ratios for a selection of intersections, and the space mean speed of the road sections of the network. We take into account economical constraints by proposing a flexible sensor location scheme that identifies the optimal locations to measure the turning ratios. The results of the proposed methods are tested using microsimulations.

This paper is organized as follows. Section 2 defines the traffic variables and traffic evolution model that are used throughout the paper, and proposes an estimator for the density of each road of a traffic network. Section 3 discusses the location of different sensor technologies required by the estimator, and proposes a method to identify the most critical locations to instrument with sensors in order to reduce estimation error. Section 4 presents the use of simulated data to evaluate the performance of the models and algorithms described in the paper. Section 5 ends the paper with a conclusion.

2. MODEL

We define a traffic network as a directed graph $\mathcal{G} = \{\mathcal{N}, \mathcal{E}\}$ where the nodes $\mathcal{N} \subset \mathbb{N}$ correspond to intersections and junctions, and the edges $\mathcal{E} \subset \mathcal{N} \times \mathcal{N}$ correspond to road sections. Additionally, for every road section i, there are associated parameters such as the road length ℓ_i, number of lanes Γ_i, and maximum velocity $v_i^{\max}$.

The traffic state refers to the collection of road densities, inflows and outflows for all roads, which we denote with vectors $\boldsymbol{\rho}(t), \boldsymbol{\varphi}^{\mathrm{in}}(t), \boldsymbol{\varphi}^{\mathrm{out}}(t) \in \mathbb{R}^{|\mathcal{E}|}$. Traffic dynamics are governed by the conservation law

$$\frac{\mathrm{d}}{\mathrm{d}t}\boldsymbol{\rho}(t) = L^{-1}(\boldsymbol{\varphi}^{\mathrm{in}}(t) - \boldsymbol{\varphi}^{\mathrm{out}}(t)) \tag{1}$$

where L is a diagonal matrix containing the road lengths, i.e., $L = \mathrm{diag}(\boldsymbol{\ell})$.

Intersections are modeled as 0 dimensional points that do not store vehicles. To model the exchange of inflows and outflows of the different roads at the intersections we use the parameters called turning ratios. Let $\mathcal{I}(n)$ be the set of incoming roads to some intersection $n \in \mathcal{N}$ and $\mathcal{O}(n)$ be the set of outgoing roads from n. A turning ratio $r_{i,j}$ for $i \in \mathcal{I}(n)$ and $j \in \mathcal{O}(n)$ defines the proportion of vehicles exiting i that enters j. As intersections do not store vehicles, then the conservation of density implies that

$$\sum_{j \in \mathcal{O}(n)} r_{i,j} = 1 , \quad \forall n \in \mathcal{N} \quad \forall i \in \mathcal{E} \setminus \mathcal{E}^{\mathrm{out}} \tag{2}$$

where $\mathcal{E}^{\mathrm{out}}$ are outgoing roads at the boundary of the network, hence have no downstream roads. Let $R \in \mathbb{R}^{|\mathcal{E}| \times |\mathcal{E}|}$ be the turning ratio matrix with elements $r_{i,j}$. If there is no connection between roads i, j, then $r_{i,j} = 0$. The input flows of each section can be expressed as a linear combination of the output flows of the preceding sections.

$$\boldsymbol{\varphi}^{\mathrm{in}}(t) = R^{\top}\boldsymbol{\varphi}^{\mathrm{out}}(t) + \boldsymbol{\varphi}^{\mathrm{ext}}(t) \tag{3}$$

where $\boldsymbol{\varphi}^{\mathrm{ext}}(t)$ corresponds to the external inflows (also known as the input demands), which are the incoming flow for the roads which are at the boundaries of the network. Combining eqs. (1) and (3), we have

$$\frac{\mathrm{d}}{\mathrm{d}t}\boldsymbol{\rho}(t) = L^{-1}(R^{\top} - \mathbb{I})\boldsymbol{\varphi}^{\mathrm{out}}(t) + L^{-1}\boldsymbol{\varphi}^{\mathrm{ext}}(t) \tag{4}$$

Define $v_i(t)$ as the space-mean speed of road i, that is, the average of the speeds of vehicles inside road i at time instant t. Denote $\mathbf{v}(t)$ as the speed vector with elements $v_i(t)$. Using the hydrodynamic relation, we can approximate the outflows as

$$\boldsymbol{\varphi}^{\mathrm{out}}(t) \approx V(t)\boldsymbol{\rho}(t) \tag{5}$$

where $V(t) = \mathrm{diag}(\mathbf{v}(t))$. This relation applies accurately when considering very short distances, or when the spatial variations in vehicle speed and density is negligible. We make the following assumption,

Hypothesis 1. The speed and density throughout a road section do not vary significantly in the spatial domain.

Therefore, (4) can be rewritten as

$$\frac{\mathrm{d}}{\mathrm{d}t}\boldsymbol{\rho}(t) = L^{-1}(R^{\top} - \mathbb{I})V(t)\boldsymbol{\rho}(t) + L^{-1}\boldsymbol{\varphi}^{\mathrm{ext}}(t) \tag{6}$$

Consider the open-loop estimator

$$\frac{\mathrm{d}}{\mathrm{d}t}\hat{\boldsymbol{\rho}}(t) = L^{-1}(\hat{R}^{\top} - \mathbb{I})\hat{V}(t)\hat{\boldsymbol{\rho}}(t) + L^{-1}\boldsymbol{\varphi}^{\mathrm{mea}}(t) \tag{7}$$

where $\hat{R}$, $\hat{V}(t)$, $\boldsymbol{\varphi}^{\mathrm{mea}}(t)$ are the measured turning ratios, road velocities, and flows, respectively. The measurement process is described in Section 3.

3. SENSOR LOCATION AND INPUT DATA

The use of the dynamic model (7) requires the knowledge of the turning ratio parameters $r_{i,j}$, the measurement of space-mean speeds $\mathbf{v}(t)$, and flow measurements. We consider the following sources of information:

3.1 Floating car data

Consider that a fraction of the vehicles in the network are equipped with devices (e.g. a GPS navigator) that periodically report to a centralized server information about the vehicles trajectory, such as its position and velocity at a given time via FCD. However, because of privacy policies, only aggregated variables and not the raw vehicles are available.

Define by $\mathcal{V}_i(t)$ the set of vehicles indexes that provide FCD that are inside road i at time t. The total number of vehicles in i cannot be estimated with this information as the penetration rate of vehicles that provide FCD is unknown. However, as the velocity of a vehicle is affected by the velocities of surrounding vehicles, this can be used to estimate the space-mean speed of the section. Let ν_α be the speed of a vehicle indexed by α. We define the aggregated speed for road section i from FCD data by

$$v_i^{\mathrm{FCD}}(t) = \frac{1}{|\mathcal{V}_i(\tau)|} \sum_{\alpha \in \mathcal{V}_i(t)} \nu_\alpha(t) \tag{8}$$

We assume in what follows that the aggregated speeds are available for all roads. In the case where the information is not available for some roads due to a lack of reporting vehicles, we use the value of the maximum speed (or speed limit) $v^{\max}$. Moreover, as the FCD speeds are direct measurements of the space-mean speed, we consider

$$V(t) = \hat{V}(t) \tag{9}$$

3.2 Stationary counting sensors

Counting sensors such as cameras, induction loops, radar, and others, are the most commonly used way to obtain traffic information. These sensors are placed in a fixed position in a road section, and collect information of the vehicles passing through that point. The collected data varies according to the technology, but generally variables such as length, speed, and time of passage are recorded. In some applications, technical constraints allow only aggregated data to be accessible, such as the total number of vehicles observed during a time interval, from which flow in the road section can be estimated.

We consider that sensors are located in the incoming roads at the boundary of the network, such that the external flows $\boldsymbol{\varphi}^{\text{ext}}(t)$ are measured directly,

$$\boldsymbol{\varphi}^{\text{mea}}(t) = \boldsymbol{\varphi}^{\text{ext}}(t) \tag{10}$$

3.3 Turning ratio measurements

Turning ratio information can be obtained by different ways. One option is the use of vehicle identifier sensors such as Blutooth or WiFi taggers, and license plate readers can be located at the incoming and outgoing roads of intersections, such that an approximate count of the number of vehicles making each turn is obtained. Another option is manual collection of data during time periods, and extrapolate the recollected data for all times. However, using any of these methods for all intersections is unfeasible, as budgetary limits can be surpassed in networks with more than a few intersections.

Another approach is to use a priori values for these parameters, which are calculated using only the physical characteristics of the network with ad hoc heuristics, and can be used as working values to provide estimates. This however introduces large sources of error, as the a priori values can be very far from the real parameters. Nevertheless, this error can be reduced by measuring a selection of intersections.

Suppose that a limited number of sensors are available. The selection of intersections should be done optimally to minimize the error in density estimation caused by deviations between the real and estimated turning ratios. For this, we propose a method to identify the intersections that generate the highest error given some perturbations in its turning ratios.

Estimation error   Let $\hat{r}_{i,j}$ be the a priori value proposed for some turning ratio. Let the deviation between this and the actual value be given by $\xi_{i,j}$ such that,

$$\hat{r}_{i,j} = r_{i,j} + \xi_{i,j} \tag{11}$$

The deviations $\xi_{i,j}$ will cause an error in the state estimation

$$\mathbf{e}(t) = \boldsymbol{\rho}(t) - \hat{\boldsymbol{\rho}}(t). \tag{12}$$

Define $\hat{R}$ and Ξ as matrices with elements $\hat{r}_{i,j}$ and $\xi_{i,j}$, respectively. Note that $\hat{R} = R + \Xi$. To quantify the sensitivity of the turning ratios in the error, we neglect the effects of time variations of the external flows and velocities, that is $V(t) = V$ and $\boldsymbol{\varphi}^{\text{ext}}(t) = \boldsymbol{\varphi}^{\text{ext}}$.

We want to express the effect of the turning ratio perturbations Ξ in the reconstruction error $\mathbf{e}(t)$. To simplify the notation, let $M = (\mathbb{I} - R^{\top})V$ and $\hat{M} = (\mathbb{I} - \hat{R}^{\top})V$, such that $\hat{M} = M - \Xi^{\top}V$. Under the assumption that section speeds are constant, the dynamics (6) and (7) become time-invariant, for which a closed-form solution is known,

$$\boldsymbol{\rho}(t) = \mathrm{e}^{-L^{-1}Mt}\boldsymbol{\rho}(0) + \left(\int_0^t \mathrm{e}^{-L^{-1}M\tau}\mathrm{d}\right)L^{-1}\boldsymbol{\varphi}^{\text{ext}}$$
$$\hat{\boldsymbol{\rho}}(t) = \mathrm{e}^{-L^{-1}\hat{M}t}\hat{\boldsymbol{\rho}}(0) + \left(\int_0^t \mathrm{e}^{-L^{-1}\hat{M}\tau}\mathrm{d}\right)L^{-1}\boldsymbol{\varphi}^{\text{ext}} \tag{13}$$

Therefore, the error can be written explicitly as

$$\mathbf{e}(t) = e^{-L^{-1}Mt}\boldsymbol{\rho}(0) - e^{-L^{-1}\hat{M}t}\hat{\boldsymbol{\rho}}(0)$$
$$+ \int_0^t \left(e^{-L^{-1}M\tau} - e^{-L^{-1}\hat{M}\tau}\right)\mathrm{d}\tau L^{-1}\boldsymbol{\varphi}^{\text{ext}} \tag{14}$$

In Rodriguez-Vega et al. (2019), we showed that $\mathbb{I} - R^{\top}$ is an invertible M-matrix, with all eigenvalues having positive real parts. Therefore, it can be shown that $-L^{-1}M$ has eigenvalues with negative real parts, so it is a stable matrix. Thus, the asymptotic error is

$$\mathbf{e} = \lim_{t\to\infty} \mathbf{e}(t) = (M^{-1} - \hat{M}^{-1})\boldsymbol{\varphi}^{\text{ext}} \tag{15}$$

where we have used the facts that the exponential function of a stable matrix goes to zero as time goes to infinity, and that

$$\int_0^\infty e^{At}\mathrm{d}t = -A^{-1} \tag{16}$$

for any stable matrix A.

Sensitivity of turning ratio deviations   Suppose that the deviations $\xi_{i,j}$ are small, and that we want to calculate the error resulting from small nudges in a single value,

$$\frac{\partial\mathbf{e}}{\partial\xi_{i,j}} = \frac{\partial}{\partial\xi_{i,j}}\left((M^{-1} - \hat{M}^{-1})\boldsymbol{\varphi}^{\text{ext}}\right)$$
$$= -\left(\frac{\partial}{\partial\xi_{i,j}}\hat{M}^{-1}\right)\boldsymbol{\varphi}^{\text{ext}} \tag{17}$$

Consider the following theorem.

Theorem 2. (Magnus and Neudecker (2019)) Let $A(t)$ be an invertible matrix that depends on a scalar parameter t. Then,

$$\frac{\mathrm{d}A^{-1}}{\mathrm{d}t} = -A^{-1}\frac{\mathrm{d}A}{\mathrm{d}t}A^{-1} \tag{18}$$

Using Theorem 2, (17) can be written as

$$\frac{\partial\mathbf{e}}{\partial\xi_{i,j}} = \hat{M}^{-1}\frac{\partial\Xi^{\top}}{\partial\xi_{i,j}}V\hat{M}^{-1}\boldsymbol{\varphi}^{\text{ext}} \tag{19}$$

Assume that the turning ratio deviations are independent from each other. Thus,

$$\frac{\partial\Xi^{\top}}{\partial\xi_{i,j}} = \mathbf{u}_j\mathbf{u}_i^{\top} \tag{20}$$

where $\mathbf{u}_i$ is the i-th column of the identity matrix of suitable dimensions. Hence,

$$\frac{\partial\mathbf{e}}{\partial\xi_{i,j}} = \hat{M}^{-1}\mathbf{u}_j\mathbf{u}_i^{\top}V\hat{M}^{-1}\boldsymbol{\varphi}^{\text{ext}} \tag{21}$$

Selection of intersections   Consider an intersection $n \in \mathcal{N}$ with incoming roads $\mathcal{I}(n)$ and outgoing roads $\mathcal{O}(n)$. Let $\boldsymbol{\xi}_i = \{\xi_{i,j}\}_{j\in\mathcal{O}(n)}$ for each $i \in \mathcal{I}(n)$. To quantify the effect of the perturbations $\xi_{i,j}$ on the error $\mathbf{e}$ we propose the following procedure:

(1) Calculate the Jacobian matrix

$$J_i = \frac{\partial \mathbf{e}}{\partial \boldsymbol{\xi}_i} \qquad (22)$$

for each incoming road $i \in \mathcal{I}(n)$.

(2) Calculate the error "energy" due to perturbations in the turning ratios of i using the Frobenius norm of the Jacobian,

$$||J_i||_F^2 = \sum_{k \in \mathcal{E}} \sum_{j \in \mathcal{O}(n)} \left(\frac{\partial e_k}{\partial \xi_{i,j}} \right)^2. \qquad (23)$$

(3) Calculate the intersection weight as the total error energy due to its incoming roads,

$$w_n = \sum_{i \in \mathcal{I}(n)} ||J_i||_F^2 \qquad (24)$$

(4) Locate the available sensors in intersections with the highest values of w_n.

Note that the intersection weight can be simplified to

$$w_n = \sum_{i \in \mathcal{I}(n)} \sum_{j \in \mathcal{O}(n)} \sum_{k \in \mathcal{E}} \left(\sum_{p \in \mathcal{E}} \hat{M}_{k,j}^{-1} \hat{M}_{i,p}^{-1} v_i \varphi_p^{\text{ext}} \right)^2 \qquad (25)$$

This heuristic procedure is a greedy approach as it assumes that deviations in the turning ratio values are independent from each other.

4. SIMULATION AND VALIDATION

To evaluate the performance of the estimator, we consider a zone of downtown Grenoble, France, as seen in Fig. 1. The traffic state was obtained by simulating vehicle traces using the well-known microscopic traffic simulator Aimsun presented in Barceló and Casas (2005). This software models the position, speed and acceleration of each vehicle according to the interaction with the other vehicles in each section and intersection. The real network layout was recreated in Aimsun as shown in Fig. 2. The layout contains information about the number of lanes, speed limit, direction, possible turns at intersections, and length. **Note:** the simulated layout does not contain traffic lights.

Fig. 1. Traffic network in Downtown Grenoble.

Fig. 2. Simulated layout of the Grenoble downtown zone in Aimsun.

To run the simulation, an arbitrary but realistic time-varying flow profile was applied at the network incoming boundaries. The turning ratios were set arbitrarily using the following formula

$$\hat{r}_{i,j} = \frac{v_j^{\max} \Gamma_j}{\sum_{k \in \mathcal{O}(n)} v_k^{\max} \Gamma_k} \qquad (26)$$

where Γ_i is the number of lanes of road i. This heuristic formula is based on the intuition that roads with higher capacity receive a higher vehicle count.

As outputs of the simulation, the position and speed of all vehicles were recollected, at each time instant. To deploy the estimator (7), average road speeds where calculated using (8) directly from vehicle traces. The input flows at the network boundaries $\boldsymbol{\varphi}^{\text{ext}}(t)$ where also calculated directly by counting the number of vehicles entering these roads during a time interval of 10 minutes. For validation, the ground-truth density of road i is calculated as the average number of vehicles in the road during a time interval

$$\rho_i(t) = \frac{1}{\ell_i \Delta t} \int_{t-\Delta t}^{t} |\mathcal{V}_i(\tau)| \mathrm{d}\tau. \qquad (27)$$

Furthermore, the ground-truth flow for road i is obtained from counting the number of vehicles that exited the road during the time interval Δt.

First, we consider the case where all turning ratios are known, $\hat{R} = R$. Figure 3 shows the evolution of the real and estimated densities for one particular road of the network. For this road, the density estimates follow closely the real values, whereas the flow is underestimated. In both cases, the real values present peaks of high variations, which are due to the effect of individual vehicle behavior, which are unable to be captured by the macroscopic model in Section 2. For evaluation, we consider the metrics Mean Error (ME) and Relative Mean Error (RME) for road i, defined as

$$\text{ME}_i^{\boldsymbol{\rho}} = \frac{1}{T} \left| \int_0^T (\rho_i(t) - \hat{\rho}_i(t)) \mathrm{d}t \right| \qquad (28)$$
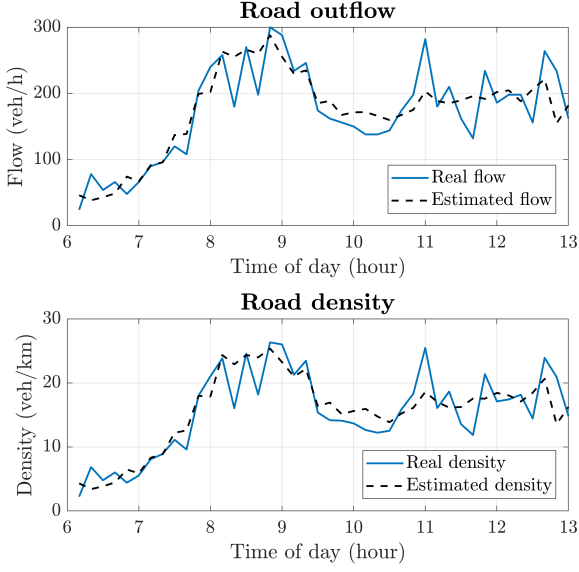
Fig. 3. Time series for the trajectories of the real and estimated density and flow for one road.

$$\mathrm{RME}_i^{\boldsymbol{\rho}} = \frac{\mathrm{ME}_{\boldsymbol{\rho}}}{\dfrac{1}{T}\displaystyle\int_0^T \rho_i(t)\mathrm{d}t} \tag{29}$$

which measure the deviation between the mean trajectories of the real and estimated quantities, and the metrics Absolute Error (AE) and Relative Absolute Error (RAE), defined as

$$\mathrm{AE}_i^{\boldsymbol{\rho}} = \frac{1}{T}\int_0^T |\rho_i(t) - \hat{\rho}_i(t)|\mathrm{d}t \tag{30}$$

$$\mathrm{RAE}_i^{\boldsymbol{\rho}} = \frac{\mathrm{AE}_i^{\boldsymbol{\rho}}}{\dfrac{1}{T}\displaystyle\int_0^T \rho_i(t)\mathrm{d}t} \tag{31}$$

which measure the total error between the two trajectories, as it not only consider the difference between their means, but also the higher frequency variations of one signal respect the other.

Figure 4 shows the Cumulative Distribution Function (CDF) for the RME and RAE for flow and density. This is the percentage of roads that have an error less than
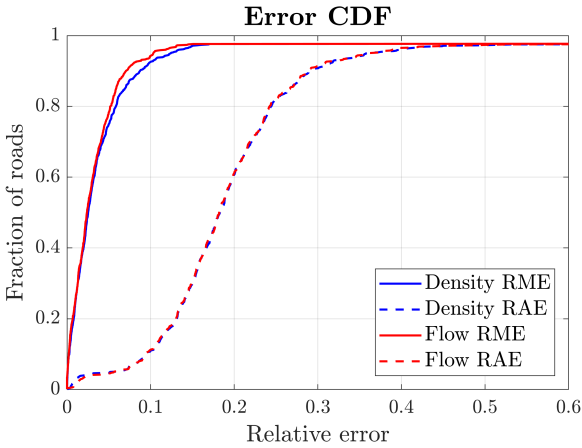

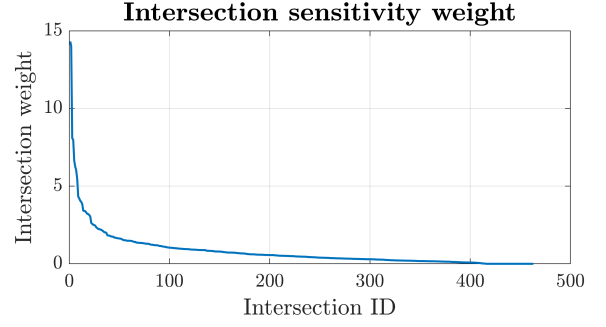
Fig. 4. CDF of the RME and RAE for flow and density.

Fig. 5. Sensitivity weight of each intersection. Intersection identifiers were sorted according to the weight.

or equal to a given value. Note from the figure that overall, the mean trajectory of the vehicles is correctly reconstructed: 90% of the roads present an error less than 8%. The AE shows the effect of the high variability of individual vehicle decisions, which increases the error to 40% for 90% of the roads. Note that the results for flow and density have approximately the same performance.

As a second scenario, we consider the case where the turning ratios in the simulation do not coincide with the estimates in eq. (26). This was done by adding noise to all turns, with a uniform distribution between -10% and 10% around the a priori estimates. To include turning ratio measurements, a set of intersections was selected using the approach described in Section 3.3.

Fig. 5 shows the distribution of the intersection sensitivity using the a priori values and maximum values of the input demands and road velocities, which are known. Note that the sensitivity weight decreases very quickly, so it is expected that diminishing returns will be observed as more sensors are located. Thus, a few number of intersections could provide a value trade-off. As an illustrating example, 20 intersections are selected such that the turning ratio for each turn is measured directly, which is approximately a 4% of the total intersections. Fig. 6 shows the location of the turning ratio sensors.
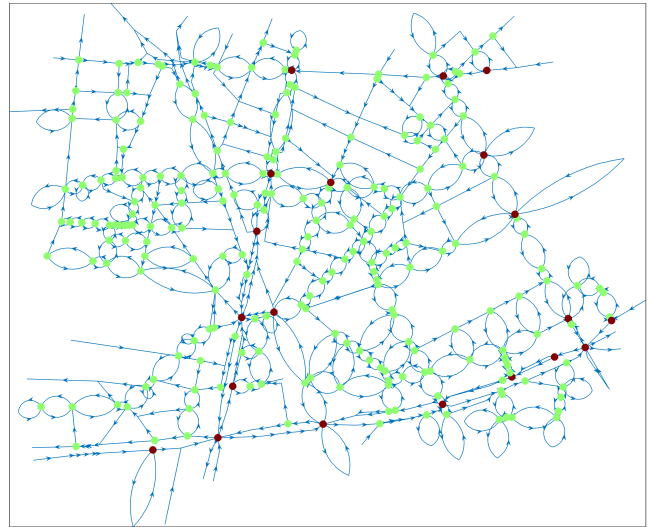

Fig. 6. Location of turning ratio sensors. Green nodes represent unmeasured intersections, whereas nodes in dark-red are the measured ones.
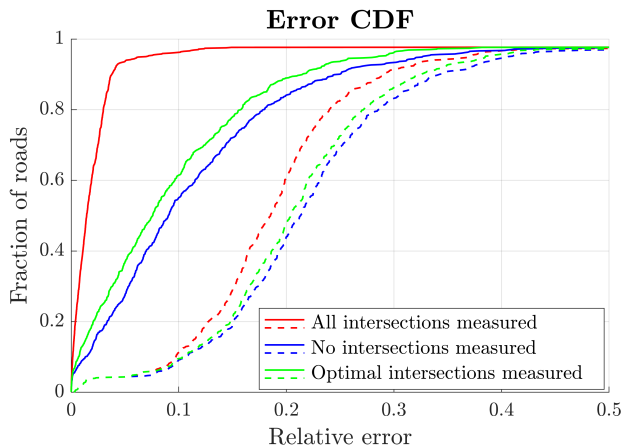
Fig. 7. Relative error for the density reconstruction according to turning ratio information.

Figure 7 shows the resulting CDF of the error in the density estimation. For comparison purposes, the results are also shown for the base case where no turning ratios in intersections are measured, and the best-case scenario where all turning ratios are known. As expected, all-ratios-known case out-performs significantly the other methods, specially in the ME. Nevertheless, this case is generally unfeasible due to practical and budgetary limitations. In contrast, the no-measurements case is the worst case scenario, and gives a lower-bound to the error. The error obtained using the proposed sensor location scheme presents an improvement of around 3% when compared with the base case.

5. CONCLUSION

In this paper, we proposed a method to estimate the dynamical evolution of flow and density in large urban traffic network by using heterogeneous data sources: counting sensors, turning ratio measurements, and floating car data. The method requires little parameters to be known, as there is no explicit modeling of the road outflows in terms of the current density, so no Fundamental Diagram is required. However, the knowledge of the turning ratios for every intersection is required. To simplify this requirement, we introduce a turning ratio sensor location scheme that takes as input a priori values for these parameters to identify the intersections for which small perturbations in the turning ratio values would generate the highest error. We tested the proposed methods using microsimulations over the city of Grenoble. The results show that the estimator performs well, as it is able to reconstruct the overall trajectory of the traffic state and has many roads presenting little errors. The approaches we propose are also flexible, as they can be applied for varying budgets. In addition, the approach allows the inclusion of new data, so the previous information can be used to improve the location of turning ratio sensors to increase the performance of the estimator.

REFERENCES

Abbott-jard, M., Shah, H., and Bhaskar, A. (2013). Empirical evaluation of Bluetooth and Wifi scanning for road transport. In *Australasian Transport Research Forum*, October, 1–14. Brisbane, Australia.

Barceló, J. and Casas, J. (2005). Dynamic Network Simulation with AIMSUN. In *Simulation Approaches in Transportation Analysis*, 57–98. Springer-Verlag, New York.

Bekiaris-Liberis, N., Roncoli, C., and Papageorgiou, M. (2016). Highway Traffic State Estimation with Mixed Connected and Conventional Vehicles. *IFAC-PapersOnLine*, 49(3), 309–314.

Bhaskar, A. and Chung, E. (2013). Fundamental understanding on the use of Bluetooth scanner as a complementary transport data. *Transportation Research Part C: Emerging Technologies*, 37, 42–72.

Canepa, E.S. and Claudel, C.G. (2017). Networked traffic state estimation involving mixed fixed-mobile sensor data using Hamilton-Jacobi equations. *Transportation Research Part B: Methodological*, 104, 686–709.

Canudas de Wit, C., Ojeda, L.L., and Kibangou, A.Y. (2012). Graph constrained-CTM observer design for the Grenoble south ring. *IFAC Proceedings Volumes*, 45(24), 197–202.

Daganzo, C.F. (1994). The cell transmission model: A dynamic representation of highway traffic consistent with the hydrodynamic theory. *Transportation Research Part B*, 28(4), 269–287.

Daganzo, C.F. (1995). The cell transmission model, part II: Network traffic. *Transportation Research Part B*, 29(2), 79–93.

Derrmann, T., Frank, R., Viti, F., and Engel, T. (2020). How Road and Mobile Networks Correlate: Estimating Urban Traffic Using Handovers. *IEEE Transactions on Intelligent Transportation Systems*, 21(2), 521–530.

Jabari, S.E. (2016). Node modeling for congested urban road networks. *Transportation Research Part B: Methodological*, 91, 229–249.

Ladino, A., Canudas-de Wit, C., Kibangou, A., Fourati, H., and Rodriguez, M. (2018). Density and flow reconstruction in urban traffic networks using heterogeneous data sources. In *IEEE European Control Conference (ECC)*, 1679–1684. Limassol, Ciprus.

Li, S., Li, G., Cheng, Y., and Ran, B. (2020). Urban arterial traffic status detection using cellular data without cellphone GPS information. *Transportation Research Part C: Emerging Technologies*, 114, 446–462.

Lighthill, M.J. and Whitham, G.B. (1955). On kinematic waves II. A theory of traffic flow on long crowded roads. *Proceedings of the Royal Society of London. Series A. Mathematical and Physical Sciences*, 229(1178), 317–345.

Lovisari, E., Canudas-de Wit, C., and Kibangou, A.Y. (2016). Density/Flow reconstruction via heterogeneous sources and Optimal Sensor Placement in road networks. *Transportation Research Part C: Emerging Technologies*, 69, 451–476.

Magnus, J.R. and Neudecker, H. (2019). *Matrix Differential Calculus with Applications in Statistics and Econometrics*. 3rd edition.

Mihaylova, L., Boel, R., and Hegyi, A. (2007). Freeway Traffic Estimation Within Particle Filtering Framework. *Automatica*, 43(2), 290–300.

Richards, P.I. (1956). Shock Waves on the Highway. *Operations Research*, 4(1), 42–51.

Rodriguez-Vega, M., Canudas-de Wit, C., and Fourati, H. (2019). Location of turning ratio and flow sensors for

flow reconstruction in large traffic networks. *Transportation Research Part B: Methodological*, 121, 21–40.

Rostami Shahrbabaki, M., Safavi, A.A., Papageorgiou, M., Setoodeh, P., and Papamichail, I. (2020). State estimation in urban traffic networks: A two-layer approach. *Transportation Research Part C: Emerging Technologies*, 115, 102616.

Seo, T., Bayen, A.M., Kusakabe, T., and Asakura, Y. (2017). Traffic state estimation on highway: A comprehensive survey. *Annual Reviews in Control*, 43, 128–151.

Takenouchi, A., Kawai, K., and Kuwahara, M. (2019). Traffic state estimation and its sensitivity utilizing measurements from the opposite lane. *Transportation Research Part C: Emerging Technologies*, 104, 95–109.

Tampère, C.M. and Immers, L.H. (2007). An extended Kalman filter application for traffic state estimation using CTM with implicit mode switching and dynamic parameters. In *IEEE Intelligent Transportation Systems Conference*, 209–216. Seattle, USA.

Treiber, M. and Kesting, A. (2013). *Traffic flow dynamics: Data, models and simulation*. Springer Berlin Heidelberg, Berlin, Heidelberg.

Wright, M. and Horowitz, R. (2016). Fusing loop and GPS probe measurements to estimate freeway density. *IEEE Transactions on Intelligent Transportation Systems*, 17(12), 3577–3590.